Engineering Structures 199 (2019) 109663

Contents lists available at ScienceDirect

Engineering Structures

journal homepage: www.elsevier.com/locate/engstruct

# Residual drift mitigation for bridges retrofitted with buckling restrained braces or self centering energy dissipation devices

A. Upadhyay, C.P. Pantelides*, L. Ibarra

*Dept. of Civil and Environmental Engineering, University of Utah, Salt Lake City, UT 84112, United States*

ARTICLE INFO

*Keywords:*
Bridge
Buckling restrained brace
Earthquakes
Reinforced concrete
Retrofit
Self centering brace

ABSTRACT

A three-column reinforced concrete bridge bent that did not have reinforcement details necessary to provide adequate load capacity and displacement ductility was evaluated under seismic excitations. Two retrofit methods for improving its seismic performance were examined: (i) Buckling Restrained Braces (BRBs), and (ii) Self Centering Energy Dissipation devices (SCEDs). The numerical model of the bridge bent was validated with previous in-situ quasi-static experiments of a full-scale bent. The BRB inelastic behavior was modeled using isotropic and kinematic strain hardening properties. Flag-shaped hysteresis with slip deformation and bearing were used to model the SCED. The numerical models of the BRB and SCED were validated with full-scale experiments of the brace members. Nonlinear time-history analysis was carried out using far-field and pulse-type ground motion sets to evaluate the seismic performance of the as-built and retrofitted bridge bents in the transverse direction. The performance limit states were defined using HAZUS criteria. Incremental dynamic analysis (IDA) was implemented to evaluate the performance of the two retrofit methods up to the collapse limit state. The results show that a retrofit with either BRBs or SCEDs improves the seismic performance of the bridge bent by decreasing drift ratio demands, and reducing the maximum steel and concrete column strains. The BRB and SCED braces reduce damage to the concrete columns by dissipating a significant portion of the input seismic energy. SCED retrofit reduces the bridge bent residual drift ratio under strong earthquakes to acceptable levels; this improves post-earthquake serviceability, increases bridge resilience and keeps repair costs low. Bridge bent peak and residual drift ratio demands were found to be higher under far-field ground motions compared to pulse-type ground motions.

## 1. Introduction

Recent surveys of U.S. highway bridges show that 24% percent of the 607,708 bridges are structurally deficient or functionally obsolete [1]. Many bridges located in high seismic regions may suffer unrepairable damage or collapse during the design basis earthquake (DBE). Damage in bridges occurs due to superstructure movement, joint failure, column damage due to shear or flexural failure, and abutment failure [2–4]. After the 1989 Loma Prieta Earthquake, more than 2000 bridges were retrofitted using conventional methods. After the 1994 Northridge earthquake, 231 bridges were repaired for various damage states. About 75% of the total estimated repair cost was spent on repair or reconstruction of collapsed bridges, which were 2.5% of the damaged bridges [5]. After the 1995 Kobe earthquake, seismic retrofit methods, such as steel jacketing and infill walls between columns, were implemented. Retrofitted bridges showed better seismic performance during the 1994 Northridge Earthquake, and the 2011 Tohoku Earthquake [4,6]. However, significant structural damage still occurred when bridges underwent large earthquake-induced displacements. Although retrofit costs are lower than reconstruction costs, serviceability is still a major concern during bridge repair [7].

The use of Buckling Restrained Braces (BRBs) in bridge structures to dissipate seismic energy has been investigated in recent years. El-Bahey and Bruneau [8] considered BRBs as structural fuses for seismic retrofit of bridge bents. Upadhyay et al. [9] used a model of a curved bridge to show that BRBs can reduce girder displacements and prevent pounding damage at the abutments. Use of BRBs in multi-column bridge bents for seismic retrofit has been studied experimentally and numerically [10–13]. Wang et al. [13] found that BRBs can redistribute and dissipate energy, reducing the seismic drift and potential failure of concrete columns and abutment shear keys. BRBs show an unbalance of 5–30% between axial compression and tension strength, caused by steel core-concrete friction during compression cycles. Moreover, the BRB steel core carries large residual strains after yielding, leading to

* Corresponding author.
*E-mail address:* c.pantelides@utah.edu (C.P. Pantelides).

https://doi.org/10.1016/j.engstruct.2019.109663
Received 28 November 2018; Received in revised form 27 August 2019; Accepted 9 September 2019

permanent deformations. Fahnestock [14,15] conducted hybrid experimental studies on a multi-story steel building equipped with BRBs and recorded large residual inter-story drifts (0.013 rad) for DBE level earthquakes. Similar BRB frame behavior has been reported from numerical studies of multi-story steel buildings while comparing the performance with Self-Centering Energy Dissipation devices [16–18]. Self-centering energy dissipation devices are more desirable in this respect. To prevent large residual deformations, application of a new self-centering buckling restrained brace (SC-BRB) in dual-column concrete box-girder bridge piers was investigated by Dong et al. [19]; a performance comparison showed that there are significant advantages of SC-BRBs over BRBs in mitigating residual drifts in bridges with good seismic detailing. Several types of SCEDs have been developed in recent years [18–23].

A statistical comparison of the seismic performance of a bridge bent retrofitted using either BRBs or SCEDs is presented. The main purpose of the BRB or SCED braces is to mitigate bridge bent residual drifts. A probabilistic analysis is carried out for the first time using Incremental Dynamic Analysis (IDA) to evaluate the residual drift and collapse capacity of the retrofitted bridge bent.

## 2. Description of bridge structure

A three-column bent of a reinforced concrete bridge tested in-situ by Pantelides et al. [24–29] was used as the base case. The bridge was designed for gravity and wind loads but not for seismic loads; it was constructed in 1963, in Salt Lake City, UT as part of the I-15 corridor. The pile cap-to-pile connections of the bent had inadequate foundation fixity and a grade beam was constructed to connect the three pile caps. Columns, beams, and beam-to-column joints were retrofitted with Carbon Fiber Reinforced Polymer (CFRP) jackets and tested under quasi-static cyclic loads [24]. Fig. 1 shows an elevation of bridge bent #5S [29] along with cross-sectional details. The bridge bent consisted of three columns with a 7.310 m clear height and section size of 0.914 × 0.914 m. The columns were 7.260 m apart on center, and the cap beam cross-section was 0.914 × 1.219 m. The columns were supported on 0.91 m thick pile caps. The two exterior pile caps were supported on four 0.30 m diameter concrete filled steel piles, 18.30 m deep; the interior pile cap was supported on five similar piles. High strength steel anchored bars were installed to strengthen the pile-to-pile cap connections as part of the previous experiments [26]. The measured in-situ compressive strength of the concrete was $f'_c$ = 34 MPa, and the yield strength of the longitudinal reinforcement was $f_y$ = 336 MPa. The columns were reinforced with sixteen 32 mm longitudinal steel bars and 13 mm single hoops spaced at 305 mm. The hoop spacing and seismic hook extensions did not meet current AASHTO design criteria, and the columns lacked confinement in the plastic hinge region.

### 2.1. Numerical modeling

A non-linear model of the bent was created using Opensees software, as shown in Fig. 2 [30]. The columns and cap beam were modeled using *nonlinear force-based beam column elements* with fiber sections discretized at four integration points to capture the component's nonlinear response. The square column cross-section had 30 fibers in each direction; the cover concrete was modeled using *Concrete04* material to simulate total loss of compressive strength after concrete crushing, which leads to spalling. The core concrete was modeled using *Concrete02* material which has some residual strength once the crushing limit is reached. The column reinforcement was modeled with *Reinforcing Steel Material* [31] which can incorporate low cycle fatigue based on Miner's rule and post-yield buckling of the steel bars [32]. Based on hoops spaced at 305 mm and 32-mm diameter longitudinal bars, the reinforcement slenderness ratio ($L_{SR}$ = 305/32 = 9.53) was very high, making it vulnerable to rebar buckling once the cover concrete had spalled. Shear strength of the columns was included using the *section aggregator* in OpenSees.

It was assumed that the cap beam-to-column and column-to-pile cap joints were strong enough to withstand the shear forces; thus, no material degradation at the joints was considered. The deck load of 3876 kN was applied at the top nodes of the three columns. Each column had a dead weight of 144 kN that was included in the model as a concentrated load divided equally on the top and bottom nodes of the columns. The column-to-cap beam joints were modeled with rigid elements, as shown in Fig. 2. The columns were assumed as fixed at the base due to the seismic retrofit implemented at the pile-to-pile cap connections and the grade beam connecting the three pile caps [24,29].

One of the original bridge bents was seismically retrofitted with CFRP jackets [24,27,28]. In this study, two alternative seismic retrofit schemes are examined: (a) installing two BRB braces, or (b) installing two SCEDs, as shown in Fig. 1. An important component of the seismic retrofit is the connection of the brace to the structure, given that the braces provide additional stiffness, which increases the seismic forces. The brace force is transferred to the reinforced concrete frame leading to higher shear demand at the brace-to-frame connection. Mahrenholtz et al. [33] have shown that BRB installation in a weak reinforced concrete frame may lead to severe shear damage to the column. During the retrofit process, it is important to choose a lateral load resisting system that prevents damage to existing structural components. Hence, in the proposed retrofit scheme, it was decided to transfer seismic forces in the braces to the cap beam and foundation by leaving a gap of 25 mm between gusset plates and column faces (Fig. 1). This connection type has been used successfully in an experimental study of a BRB retrofit of a two-column bridge bent [10,11]. The brace-to-gusset plate and gusset plate-to-concrete connections were assumed to remain elastic.

The seismic retrofit design concept, shown in Fig. 3, consists of idealized bilinear pushover curves for the bare bent, braces and retrofitted bent. The braces are designed to yield earlier than the concrete frame, working as structural fuses, enhancing the system's lateral load carrying capacity and displacement ductility. This early yielding mechanism enables the retrofitted structure to dissipate seismic energy through hysteretic behavior of the braces, while the gravity load carrying components remain elastic. Seismic loads were calculated following ASCE 7 [34] which considers moment frames with BRBs as "dual systems". The BRBs were designed to resist 50% of the total design seismic base shear, as recommended by Wang et al. [13], based on a parametric study of the BRB core area.

### 2.2. BRB numerical model

BRBs have a steel core with a reduced area in the central section, and a larger area in the two end-sections that are connected to gusset plates. The steel core is confined by a steel tube filled with mortar; a thin air gap is present between the mortar and the steel core, as shown in Fig. 4(a). The BRBs in this research were assumed to have a length ratio (LR), i.e. ratio of reduced-area core length to work point length equal to 0.55. Based on the design procedure, two BRBs with a reduced core area of the core equal to 1450 $mm^2$ and core length of 5670 mm were implemented. The BRB components were modeled utilizing the Giuffré-Menegotto-Pinto (*Steel02*) material model in Opensees which includes isotropic and kinematic hardening. BRB's hysteretic response is a combination of kinematic and isotropic hardening behavior. This behavior is caused by the contact friction of the confined concrete and the core steel plate, resulting in a compression capacity higher than the tension capacity. To capture this complex behavior, the symmetric *Steel02* material model is combined in parallel with the *Pinching4* material, using the tension and compression stress values shown in Table 1. Very small non-zero values (0.0001) were selected for the tension direction of the pinching material for numerical stability. Finally, the combination of *Steel02* and *Pinching4* material was combined with *Fatigue Material* [35] available in OpenSees to limit the otherwise infinite deformation capacity of the *Steel02* material. *Fatigue Material* is

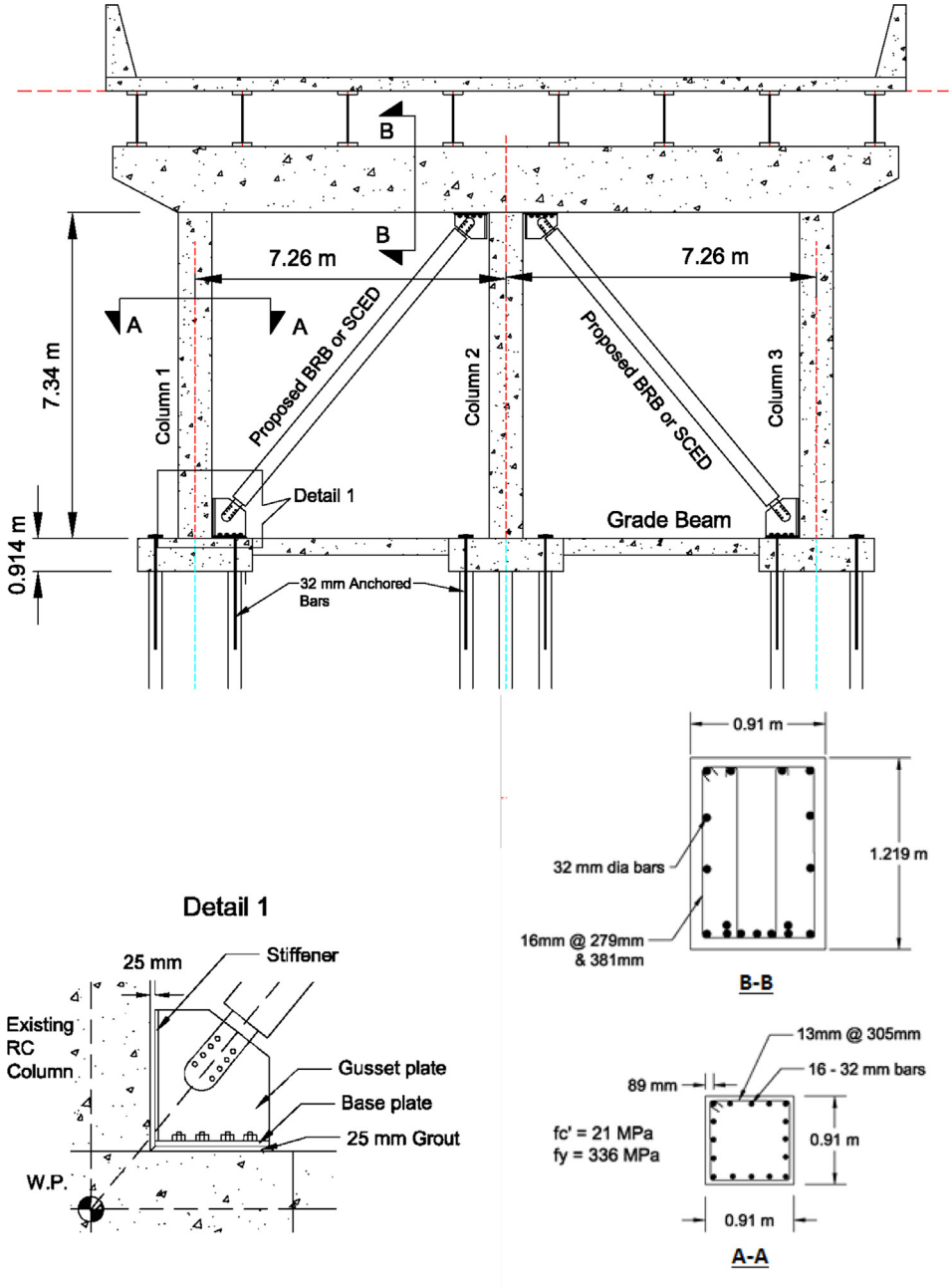


**Fig. 1.** Bridge bent elevation, brace connection and section details.

based on Miner's rule and calculates the total maximum cumulative plastic deformation in the BRB yielding core. The final BRB material model, which is a combination of *Steel02, Pinching4*, and *Fatigue Material* is assigned to a *corotational truss element* with cross-sectional area calculated by the design procedure.

Since the BRB element in the numerical model is assigned between work-point nodes, it corresponds to an equivalent BRB stiffness (Eq. (1)), which is a combination of the stiffness provided by the core and end sections, connected in series. If the BRB ends are assumed to have a much larger cross-sectional area, which makes the two end sections almost rigid, the component stiffness is mainly provided by the reduced-area steel core. The modulus of elasticity of the BRB material in the numerical model was modified to reflect the core stiffness, as per Eq. (2).

$$\frac{1}{K_{BRB}} = \frac{1}{K_{core}} + \frac{2}{K_{end}} \tag{1}$$

$$E_{wp} = E_s \frac{L_{wp}}{L_{core} + 2L_{end}\frac{A_{core}}{A_{end}}} \tag{2}$$

where $E_{wp}$ is the equivalent modulus of elasticity of the brace when modeled as a single truss element with cross-sectional area equal to the BRB core area, $E_s$ is the steel modulus of elasticity (200 GPa), $L_{wp}$ is the work-point length of the BRB, $L_{core}$ is the length of the yielding core of the BRB, $L_{end}$ is the length of the end sections of the BRB, $A_{core}$ is the cross-sectional area of the BRB yielding core, and $A_{end}$ is the cross-sectional area of the end section of the BRB. This methodology has been used in the past to successfully model the behavior of BRBs in bridge retrofits [10,11]. To calibrate the BRB component, a numerical model of a BRB quasi-static cyclic test was subjected to the cyclic axial displacement loading protocol used in the experiment [36]. The parameters in Miner's rule for *Fatigue Material* were calculated through iteration to match fatigue failure with published experimental data [36]. A comparison of the numerical and experimental hysteretic

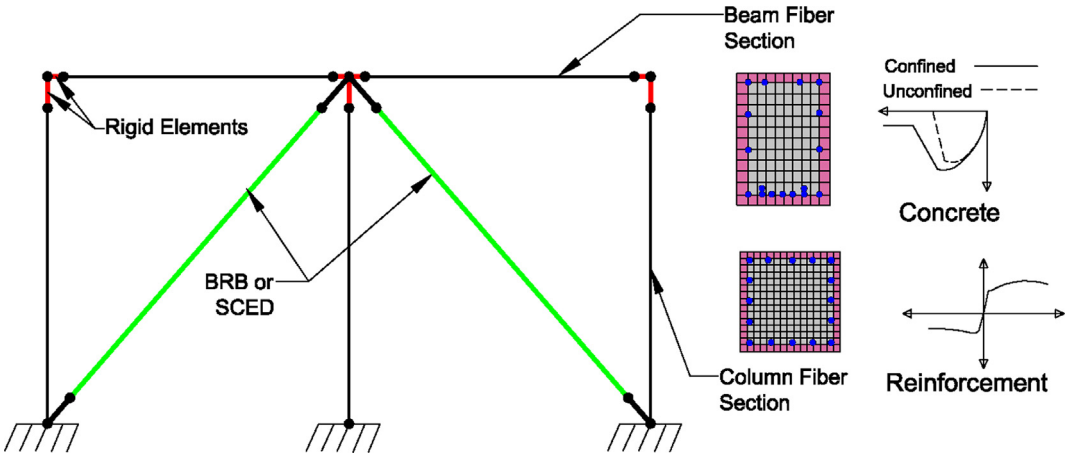


**Fig. 2.** Retrofitted bent model in OpenSees.

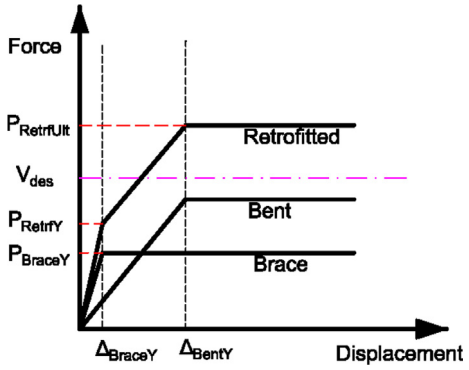


**Fig. 3.** Design concept of BRBs or SCEDs for the bridge bent.

response is presented in Fig. 5(a). It is important to compare the performance of the BRB numerical model with the BRB test in terms of initial stiffness, peak force, non-symmetric response, strain hardening behavior and cyclic fatigue failure [37,38]. The comparison between the numerical model and the BRB cyclic test was quantified in terms of percent error in predicting the strain hardening factor (ω), the compression adjustment factor (β) and hysteretic energy in each cycle. As shown in Table 2, the BRB numerical model had a 10% error in calculation of β in the first cycle, which was reduced to 1% in the 6th cycle. The BRB numerical model predicted ω with a maximum error of 3%. The percent error in cumulative hysteretic energy after the 6th cycle was 2%. The OpenSees BRB model accurately captured the BRB cyclic test behavior. The calibrated input parameters to define *Steel02, Pinching4* and *Fatigue Materials* are provided in Table 1.

**Table 1**
Calibrated input parameters for BRB modeling.

| **Steel02** | **R0** | $F_y$ | **CR1** | **CR2** | **a1** | **a2** | **a3** | **a4** |
|---|---|---|---|---|---|---|---|---|
| | 26 | 277.2 MPa | 0.91 | 0.10 | 0.045 | 1.02 | 0.55 | 1.0 |
| **Pinching4** | | **Point 1** | **Point 2** | **Point 3** | | **Point 4** | | |
| Strain | | −0.0001 | −0.00636 | −0.023 | | −0.318 | | |
| Negative Stress | | −0.016 $F_y$ | −0.032 $F_y$ | −0.201 $F_y$ | | −0.215 $F_y$ | | |
| Positive Stress | | 0.0001 | 0.0001 | 0.0001 | | 0.0001 | | |
| **Fatigue** | | $\varepsilon_o$ | ***M*** | **min** | | **max** | | |
| | | 0.191 *LR* | 0.671 | −0.035 | | 0.035 | | |

*LR* = Length ratio of BRB.

### 2.3. SCED numerical model

A schematic of an SCED brace is shown in Fig. 4(b). It consists of pretensioned tendons in two layers (outer and inner), such that one set of the pretensioned tendons is always in tension to provide recentering. Energy is dissipated by a friction device attached in parallel to the steel tubes. The initial stiffness of the brace is obtained from a combination of the stiffness of the outer and inner steel casings. The secondary stiffness is provided solely by the pretensioned tendons. The load at which the brace changes its stiffness from primary to secondary is known as the "activation point", which is equal to the static friction threshold in the friction device of the brace. Self-centering energy dissipation braces were designed using a procedure similar to the BRB design. The activation force of the SCED was assumed to be equal to the BRB yield force of 402 kN with a brace initial stiffness $K_1$ = 56,876 kN/m and a secondary stiffness $K_2 = 0.015\,K_1$. The *SelfCentering Material* model in OpenSees was used to model the SCED brace components [20]. The material can model slip of an external friction fuse, which causes non-recoverable deformation above a certain strain in the brace.

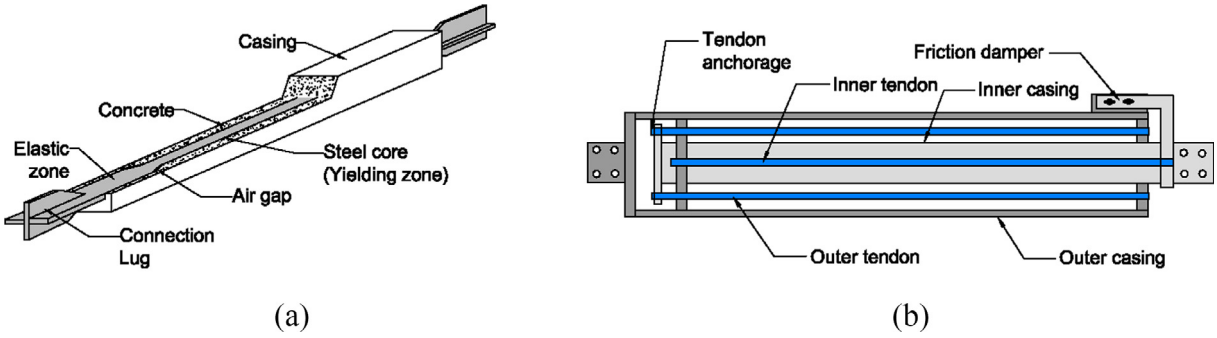


**Fig. 4.** Schematic diagram: (a) BRB; (b) SCED.

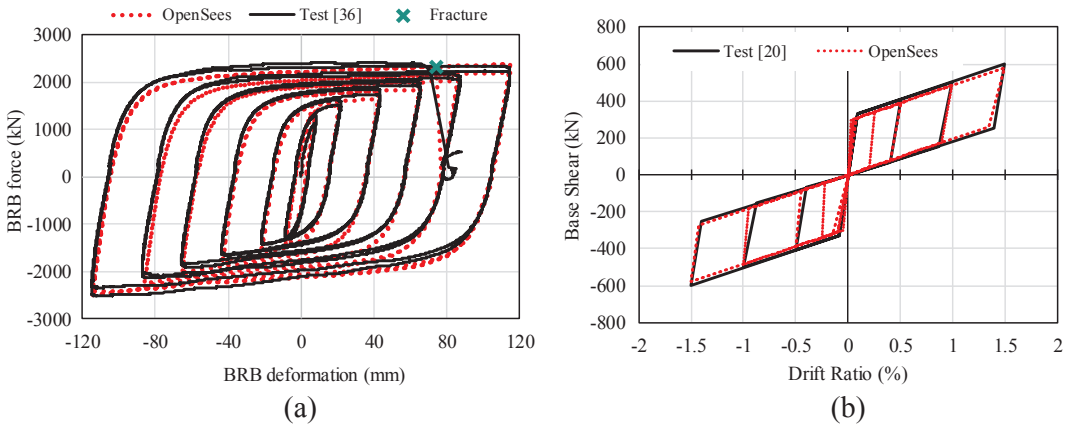


**Fig. 5.** Validation of OpenSees component model: (a) BRB; (b) SCED.

**Table 2**
Percent Error in BRB numerical model cyclic performance.

| Cycle | % Error in β | % Error in ω | % Error in Cumulative Hysteretic Energy |
|---|---|---|---|
| 1 | 10% | 3% | 15% |
| 2 | 8% | 2% | 13% |
| 3 | 7% | 2% | 8% |
| 4 | 4% | 1% | 4% |
| 5 | 1% | 1% | 2% |
| 6 | 1% | 1% | 2% |

In practice, the external friction fuse is used to limit the amount of force in the brace, since the post-activation stiffness is generally non-zero. The bearing option is used to approximately model the effect of bolt bearing in the brace or external fuse mechanism, which causes a steep increase in brace stiffness. For self-centering energy-dissipative brace simulation, this bearing effect may be used to impose a limit on slip or activation strain based on the anticipated available strain capacity of the mechanism. To calibrate the SCED material, a subassemblage test performed by Christopoulos et al. [20] was modeled in OpenSees. The initial stiffness, activation force and post-activation stiffness of the brace were adopted from Christopoulos et al. [20]. The numerical model predicted the behavior of the SCED satisfactorily (Fig. 5(b)). The slip in the brace was activated once the post-tensioned tendons reached a 1.3% tensile strain to limit excessive strain in the tendons. Brace failure was assumed to occur at 2.4% strain, which corresponds to shear failure of friction bolts in the device.

## 3. Pushover analysis

A pushover analysis was initially performed to validate the bridge bent numerical model. For validation purposes, the deck load in the numerical model was reduced to half the actual deck load to simulate real in-situ test conditions of a bridge bent retrofitted with a grade beam and high strength steel anchored bars (Bent 5S), as tested. The performance of the as-built bridge bent tested in-situ is described in [26]. As shown in Fig. 6(a), the numerical model of the bridge bent captures the behavior with sufficient accuracy. The base shear capacity of the tested bent was found to be 1956 kN at a 2.09% drift ratio, whereas the numerical model predicted the base shear capacity as 1993 kN at a 2.15% drift ratio. The numerical model could predict the first rebar yielding, spalling of the cover concrete, and buckling of column longitudinal steel bars. The first rebar yielding predicted by the numerical model was at 0.40% as compared to 0.53% drift ratio in the in-situ test. The numerical model predicted onset of rebar buckling at 3.35% drift ratio, which was close to the onset of rebar buckling observed at 3.31% drift ratio in the in-situ test.

## 4. Performance criteria

Performance assessment requires computation of engineering demand parameters (e.g., strength, drift, and ductility) that should meet specified performance targets, and correlate to damage in the structure [39]. Four damage states based on the qualitative damage descriptions of slight, moderate, extensive, and collapse based on HAZUS [40] are commonly adopted in seismic bridge assessment, as shown in Table 3. To define quantitative limit states, a mechanics-based approach correlates component deformation from curvature demands to physical damage of bridge components. The bridge bent drift ratio was selected as the quantitative damage parameter. The drift ratio was correlated to bridge bent damage to define qualitative damage states, based on the pushover analysis and damage predicted from the bridge bent analytical model. The first rebar yielding was observed at a 0.30% drift ratio which corresponds to the “slight” damage limit state or “fully operational” performance level. Spalling of the concrete was assumed when the compressive strain in the cover concrete reached ultimate strain in the fiber model. The bridge bent can be considered as “fully operational” up to this damage state. Large cover cracking or spalling accelerates loss of confinement in the plastic hinge region, given that the columns lack ductile detailing. The large spacing between confining ties quickly leads to buckling of steel bars. The bridge columns were considered to reach an extensive damage state at the onset of first rebar buckling. Based on Fig. 6(b), “life safety” and “near collapse” performance limit states occurred at drift ratios of 1.9% and 2.5%, respectively. The performance limits for retrofitted bents did not change due to the presence of BRBs or SCEDs. A summary of the performance limits, damage states and corresponding drift ratios is provided in Table 3.

## 5. Selection and scaling of ground motions

The seismic response of a structure depends on the earthquake ground motion characteristics, which are influenced by soil type, earthquake intensity and frequency content. Thus, a probabilistic seismic approach is needed, which requires nonlinear time history analyses (THAs) for a large number of ground motions. The bridge site is located approximately 12 km from the Wasatch fault in Salt Lake City. Thus, two sets of ground motions, 22 far-field (FFGMs) and 21 near-field pulse-type ground motions (PTGMs) were selected to perform nonlinear THAs. The 22 FFGMs were obtained from the FEMA P695 project [41], as shown in Table 4. The horizontal component of the selected ground motions was first matched to the spectral acceleration Sa(T1) of the Design Basis Earthquake (DBE) and the first analysis was performed. A second analysis was done by matching the selected ground motions for the Maximum Considered Earthquake (MCE), to evaluate the structure’s performance under both hazard levels. This

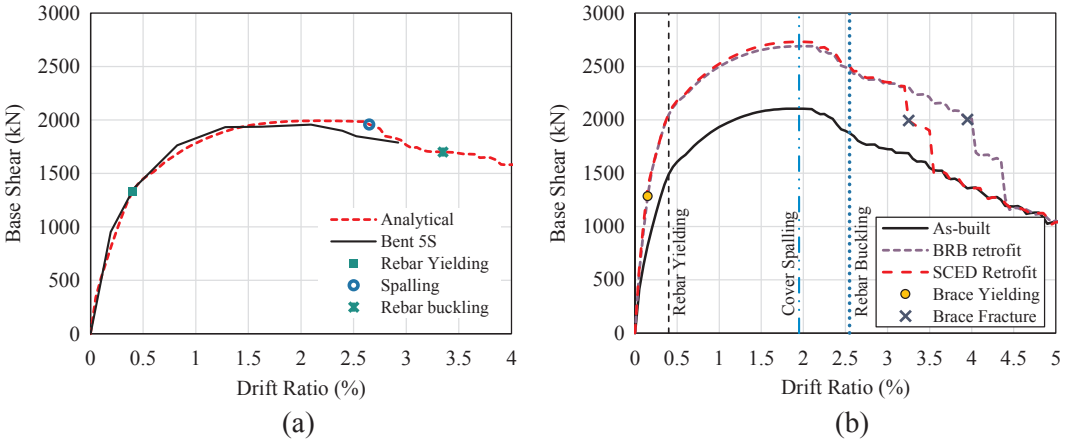


**Fig. 6.** Pushover analysis: (a) validation of numerical model; (b) comparison of as-built and retrofitted bent.

scaling process was selected to reduce variability in the output parameters. The ground motions were applied directly to the bridge pier base nodes.

The site soil can be classified as soft to stiff clay, and hence a soil site Class D is assumed with minimum and maximum shear wave velocities of 100 m/s and 310 m/s, respectively. The ASCE-7 [34] standard horizontal Design Basis Earthquake (DBE) response spectrum and Risk-Targeted MCE response spectrum for the bridge site were developed using the USGS design maps tool [42]. The Pacific Earthquake Engineering Research Center [43] strong motion database was searched for acceleration records for strike-slip and reverse/oblique fault type with shear wave velocity of the site (Vs30). The source-to-site distance was taken as the rupture ($R_{Rup}$) distance provided in the PEER NGA database.

## 6. Non-linear time history analysis

Nonlinear THAs were performed for the as-built and retrofitted bridge bent models. The effect of BRB or SCED retrofit was analyzed by subjecting the bridge bent model to FFGMs and PTGMs scaled to the site MCE level with $S_a(T_1) = 1.49$ g. In general, the as-built bridge bent experienced higher drift ratios than the bents retrofitted with BRBs or SCEDs, as observed in Fig. 7(a) and (b), which show the transverse displacement time-histories at the bent top for a representative FFGM and PTGM, respectively. As observed, BRBs and SCEDs reduce the peak drift ratio by more than 40%. The BRB retrofit resulted in reduction of peak drift ratio, but also led to large residual drift ratio when subjected to the FFGM Kobe (1995). For the PTGM Parkfield (2004), the retrofit schemes performed similarly with relatively lower residual drift ratios as compared to the representative FFGM.

Cumulative Distribution Functions (CDFs) for peak and residual drift ratio for the as-built and retrofitted bents are shown in Fig. 8. The median value of maximum drift ratio for FFGMs scaled to the MCE level was 1.50% for the as-built bridge bent, as compared to 0.63% for the bent with the BRB retrofit, and 0.70% for the SCED retrofitted bent. The probability of exceeding the "Extensive" damage state for the as-built bridge bent was 18%, which was reduced to 1% for the bent with the BRB retrofit, and 4% for the bent with the SCED retrofit, as shown in Fig. 8(a). The cumulative probability of exceeding the "Moderate" damage state was reduced from 32% for the as-built condition, to 10% for the bent with the SCED retrofit, and 5% for the bent with the BRB retrofit. Fig. 8(b) presents the residual, or permanent, drift ratio for the as-built and retrofitted bents. Vision 2000 [44] recommends the serviceability limit for residual drift ratio to be 0.5%. The cumulative probability of exceeding the 0.5% residual drift ratio under FFGMs for the as-built bridge bent was 18%, which was reduced to 7% for the BRB retrofit and close to 0% for the bridge bent retrofitted with SCEDs.

The bridge bent was also analyzed for the 21 PTGMs shown in Table 5. Fig. 8(c) and (d) show the CDFs of peak and residual drift demands, respectively, for the as-built and retrofitted bridge bents subjected to PTGMs. The median peak drift ratio for the as-built bridge bent was 1.2% under PTGMs, a 20% reduction from the 1.5% drift obtained under FFGMs; FFGMs have multiple large acceleration peaks that cause cyclic degradation in the reinforced concrete components. The probability of exceeding the "extensive" damage state was 10% for the as-built, and 2% for both the BRB and SCED retrofitted bridge bent. The probability of exceeding the "moderate" damage state was 20% for the as-built bridge bent, and 6% for the BRB and SCED retrofitted bridge bents. The probability of exceeding 0.5% residual drift (serviceability) was 13% for the as-built bridge bent while it was 3% for the BRB retrofitted and close to 0% for the SCED retrofitted bridge bent.

Interestingly, Fig. 8(a) and (c) indicate that the BRB retrofit performs slightly better regarding the peak drift than the SCED retrofit when the bridge is subjected to FFGMs, as compared to PTGMs. The BRB core undergoes cyclic strain hardening (Fig. 5(a)), gaining more resistance in each cycle, unlike the SCED behavior. This additional strength enhances the BRB retrofit performance, as shown in Fig. 9(a) and (b), keeping the median value of peak drift ratio lower than that of the SCED retrofit. Fig. 8(a) shows that the BRB retrofit performed slightly better than the SCED retrofit when subjected to far-field ground motions, and the difference in performance was found to be statistically significant, based on a one-tail t-statistics analysis. However, the difference in performance of the two retrofit schemes was not statistically significant when subjected to pulse-type ground motions (Fig. 8(c)). A null hypothesis assuming the population means of peak drift demands for the two retrofit schemes to be equal was examined. This null

**Table 3**
Quantification of performance limit states.

| Level | Limit State | Performance Level | Physical Description | Hazus Adopted Drift Ratio (%) | Vision 2000 Drift Ratio (%) |
|---|---|---|---|---|---|
| I | Slight | Fully Operational | First rebar yielding, Cracking | 0.4 | 0.5 |
| II | Moderate | Life Safety | Spalling, Exposure of column core | 1.9 | 2.0 |
| III | Extensive | Near Collapse | Major concrete cracks, Onset of rebar buckling | 2.5 | 2.5 |
| IV | Complete | Complete Collapse | Excessive deformations | – | – |

**Table 4**
Characteristics of the far-field ground motions.

| GM No. | Earthquake | | | Recording Station | Rrup (km) | PGA (g) | PGV (cm/s) |
|---|---|---|---|---|---|---|---|
| | M | Year | Name | | | | |
| 1 | 6.7 | 1994 | Northridge | Beverly Hills - Mulhol | 17.2 | 0.52 | 63 |
| 2 | 6.7 | 1994 | Northridge | Canyon Country-WLC | 12.4 | 0.48 | 45 |
| 3 | 7.1 | 1999 | Duzce, Turkey | Bolu | 12 | 0.82 | 62 |
| 4 | 7.1 | 1999 | Hector Mie | Hector | 11.7 | 0.34 | 42 |
| 5 | 6.5 | 1979 | Imperial Valley | Delta | 22 | 0.35 | 33 |
| 6 | 6.5 | 1979 | Imperial Valley | El Centro Array #11 | 12.5 | 0.38 | 42 |
| 7 | 6.9 | 1995 | Kobe, Japan | Nishi-Akashi | 7.1 | 0.51 | 37 |
| 8 | 6.9 | 1995 | Kobe, Japan | Shin-Osaka | 19.2 | 0.24 | 38 |
| 9 | 7.5 | 1999 | Kocaeli, Turkey | Duzce | 15.4 | 0.36 | 59 |
| 10 | 7.5 | 1999 | Kocaeli, Turkey | Arcelik | 13.5 | 0.22 | 40 |
| 11 | 7.3 | 1992 | Landers | Yermo Fire Station | 23.6 | 0.24 | 52 |
| 12 | 7.3 | 1992 | Landers | Coolwater | 19.7 | 0.42 | 42 |
| 13 | 6.9 | 1989 | Loma Prieta | Capitola | 15.2 | 0.53 | 35 |
| 14 | 6.9 | 1989 | Loma Prieta | Gilroy Array #3 | 12.8 | 0.56 | 45 |
| 15 | 7.4 | 1990 | Manjil, Iran | Abbar | 12.6 | 0.51 | 54 |
| 16 | 6.5 | 1987 | Superstition Hills | El Centro Imp. Co. | 18.2 | 0.36 | 46 |
| 17 | 6.5 | 1987 | Superstition Hills | Poe Road (temp) | 11.2 | 0.45 | 36 |
| 18 | 7.0 | 1992 | Cape Mendocino | Rio Dell Overpass | 14.3 | 0.55 | 44 |
| 19 | 7.6 | 1999 | Chi-Chi, Taiwan | CHY101 | 10 | 0.44 | 115 |
| 20 | 7.6 | 1999 | Chi-Chi, Taiwan | TCU045 | 26 | 0.51 | 39 |
| 21 | 6.6 | 1971 | San Fernando | LA - Hollywood Store | 22.8 | 0.21 | 19 |
| 22 | 6.5 | 1976 | Friuli, Italy | Tolmezzo | 15.8 | 0.35 | 31 |

hypothesis is rejected if the calculated probability (p-value) of the *t*-test proves to be less than the threshold value of 0.05. Assuming the null-hypothesis to be true, using two sample means $\sigma_1$ and $\sigma_2$, the sample standard deviations $S_1$ and $S_2$, and the sample sizes $N_1$ and $N_2$, the t-value can be calculated according to Eq. (3). The findings for peak drift performance of both retrofit schemes may be modified if different input parameters are considered. However, the superior performance of SCED retrofit in mitigating the residual drift ratio over the BRB retrofitted system is statistically significant and is clearly demonstrated in Fig. 8(b) and (d)

$$t = \frac{\sigma_1 - \sigma_2}{\sqrt{\frac{S_1^2}{N_1} + \frac{S_2^2}{N_2}}} \tag{3}$$

The number of ground motion records ($n$) required to have a maximum error $X$ on the estimate of the median of data which is assumed to have a lognormal distribution, with a 95% confidence, can be approximated as [45,46]:

$$n = 4S^2/X^2 \tag{4}$$

where $S$ is the standard deviation in the Engineering Demand Parameter (*EDP*) values. In this study, the peak drift ratio (%) of the bridge bent was selected as the *EDP*. For the analysis using far-field ground motions, the maximum standard deviation was 0.58 for the retrofitted bridge bent subjected to ground motions scaled to the MCE level. Assuming a maximum acceptable error $X = 0.25$ (i.e. ± 25%), a minimum of 21 ground motions are required based on Eq. (4). Since this research used 22 far-field ground motions, carefully selected by the FEMA-P695 committee to avoid repetitions, the results are in good confidence. When subjected to pulse-type ground motions scaled to MCE level, the standard deviation recorded for the BRB and SCED retrofitted bridge bents was 0.73 and 0.78, respectively. Since there is a lack of pulse-type ground motions from different earthquakes, the 21 pulse-type records used in this study may not provide results that are as reliable as those of the FFGMs.

In addition to increasing bent stiffness, BRBs and SCEDs also dissipate earthquake input energy. The energy dissipation in both retrofit systems was compared as a percentage of earthquake input energy. The earthquake input energy, kinetic energy, and damping energy were calculated using the "relative energy" concept [47]. The input energy is dissipated through various mechanisms in the structure, and can be expressed as:

$$E_{input} = E_{Kinetic} + E_{Damping} + E_{Strain} + E_{Hysteretic} \tag{5}$$

where $E_{input}$ is the earthquake input energy which is a function of the mass of the structure, $E_{Kinetic}$ is the kinetic energy stored in the structure's mass, $E_{Damping}$ is the energy dissipated by the structure

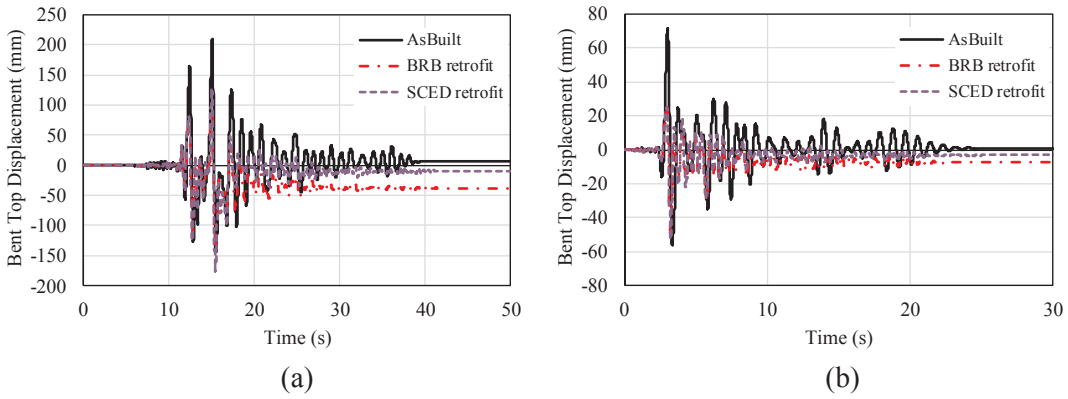


**Fig. 7.** Bent top displacement time-histories: (a) Kobe (1995) far-field ground motion; (b) Parkfield (2004) pulse-type ground motion.

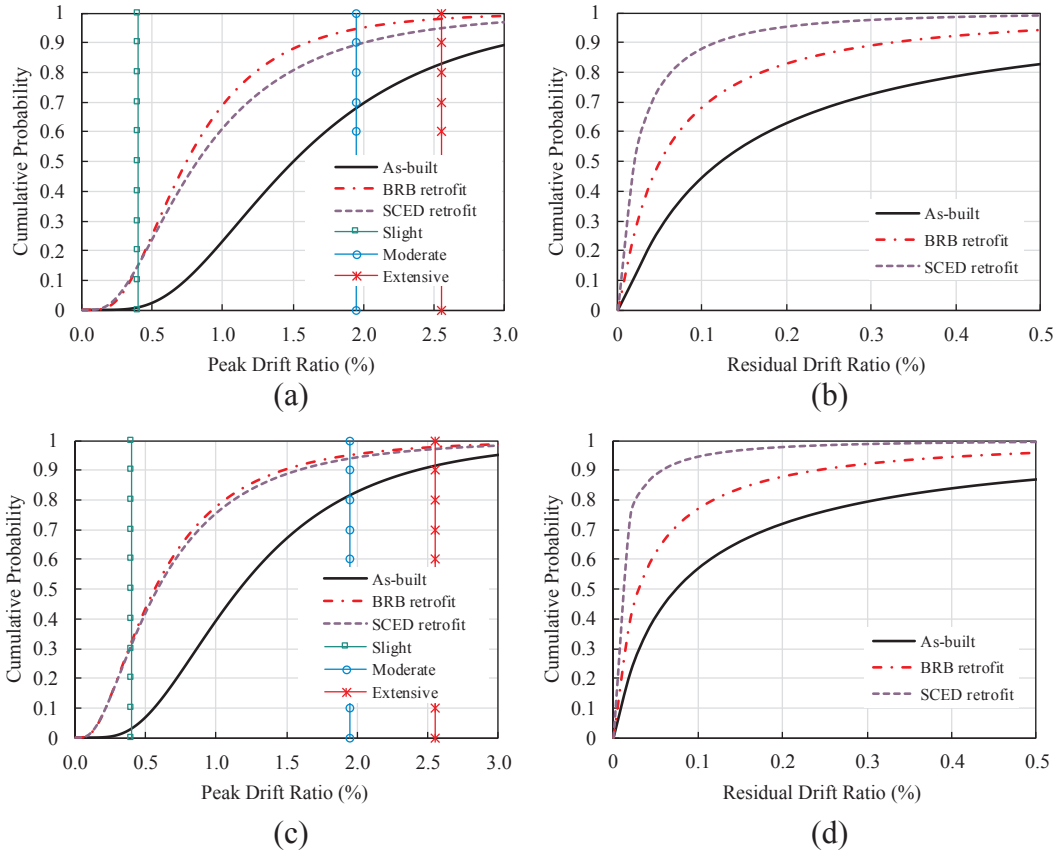


**Fig. 8.** Cumulative distribution functions for (a) peak drift under FFGMs, (b) residual drift under FFGMs, (c) peak drift under PTGMs, (d) residual drift under PTGMs scaled to MCE level.

through material damping which is the total area under the hysteresis curves, $E_{Strain}$ is the recoverable strain energy in the structure, and $E_{Hysteretic}$ is the energy dissipated by the BRBs or SCEDs. The $E_{Kinetic}$ and $E_{Strain}$ are temporary energy storage mechanisms and disappear at the end of the time-history.

It is sufficient to compare the energy dissipated by the external devices (i.e. BRBs and SCEDs) as a percentage of total input energy as shown in Fig. 10. For FFGMs, the average percentage of energy dissipated by the BRBs is 72.1%, which is higher than that of SCEDs (60.0%), because SCEDs exhibit pinching hysteretic loops, leading to higher demands. For PTGMs, however, the average percentage energy dissipated by BRBs and SCEDs is slightly closer (40.9% and 29.8%, respectively). This observation supports the results shown in Fig. 8(c) for the peak drift ratio on the bent for PTGMs. In the as-built bridge

**Table 5**
Characteristics of the pulse-type ground motions.

| GM No. | Earthquake | | | Recording Station | Rrup (km) | PGA (g) | PGV (cm/s) | $T_P$ |
|---|---|---|---|---|---|---|---|---|
| | M | Year | Earthquake Name | | | | | (s) |
| 1 | 5.7 | 1979 | Coyote Lake | Gilroy Array #2 | 9.02 | 0.26 | 31.92 | 1.46 |
| 2 | 5.7 | 1979 | Coyote Lake | Gilroy Array #3 | 7.42 | 0.26 | 29.56 | 1.15 |
| 3 | 5.7 | 1979 | Coyote Lake | Gilroy Array #6 | 3.11 | 0.42 | 44.33 | 1.23 |
| 4 | 6.5 | 1979 | Imperial Valley | Meloland Geot. Array | 0.07 | 0.53 | 92.57 | 3.42 |
| 5 | 6.5 | 1979 | Imperial Valley | El Centro Differential Array | 5.09 | 0.48 | 96.85 | 6.25 |
| 6 | 6.2 | 1984 | Morgan Hill | Coyote Lake Dam - SW Abut | 0.53 | 1.30 | 75.54 | 1.07 |
| 7 | 5.4 | 1986 | Kalamata, Greece | Kalamata (bsmt) (2nd trigger) | 5.6 | 0.26 | 78.40 | 0.78 |
| 8 | 5.8 | 1986 | San Salvador | Geotech Investig Center | 6.3 | 0.70 | 24.57 | 0.80 |
| 9 | 6.9 | 1989 | Loma Prieta | Saratoga - Aloha Ave | 8.5 | 0.51 | 79.88 | 4.57 |
| 10 | 6.7 | 1994 | Northridge | LA Dam | 5.92 | 0.99 | 45.95 | 1.61 |
| 11 | 6.7 | 1994 | Northridge | Newhall - Fire Sta | 5.92 | 0.42 | 76.09 | 1.37 |
| 12 | 6.7 | 1994 | Northridge | Sylmar - Olive View Med FF | 5.3 | 0.87 | 77.63 | 2.43 |
| 13 | 6.9 | 1995 | Kobe_ Japan | Takarazuka | 0.27 | 0.70 | 74.80 | 1.80 |
| 14 | 6.2 | 1999 | Chi-Chi, Taiwan | CHY074 | 6.2 | 0.34 | 96.54 | 2.43 |
| 15 | 6.0 | 2004 | Parkfield, CA | Parkfield - Cholame 1E | 3 | 0.44 | 118.12 | 1.33 |
| 16 | 6.0 | 2004 | Parkfield, CA | Parkfield - Cholame 2WA | 3.01 | 0.58 | 147.92 | 1.07 |
| 17 | 6.0 | 2004 | Parkfield, CA | Parkfield - Cholame 3W | 3.63 | 0.58 | 120.91 | 1.02 |
| 18 | 6.3 | 2009 | L'Aquila, Italy | V. Aterno - Centro Valle | 6.27 | 0.66 | 129.31 | 1.07 |
| 19 | 6.3 | 2009 | L'Aquila, Italy | V. Aterno -F. Aterno | 6.55 | 0.44 | 86.21 | 1.17 |
| 20 | 7.0 | 2010 | Darfield, NZ | HORC | 7.29 | 0.48 | 43.48 | 9.9 |
| 21 | 6.2 | 2011 | Christchurch, NZ | Pages Road Pumping Station | 1.98 | 0.67 | 40.11 | 4.8 |

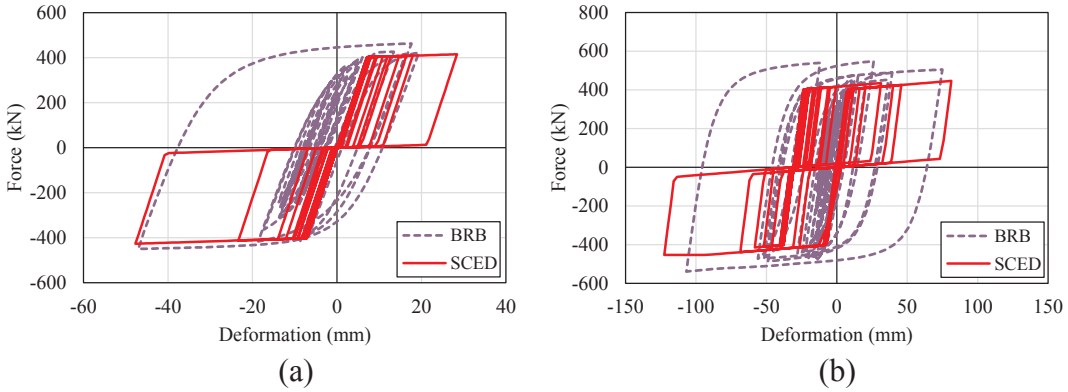


**Fig. 9.** Comparison of BRB and SCED hysteresis: (a) pulse-type (Parkfield 2007) and (b) far-field (Kobe 1995) ground motion.

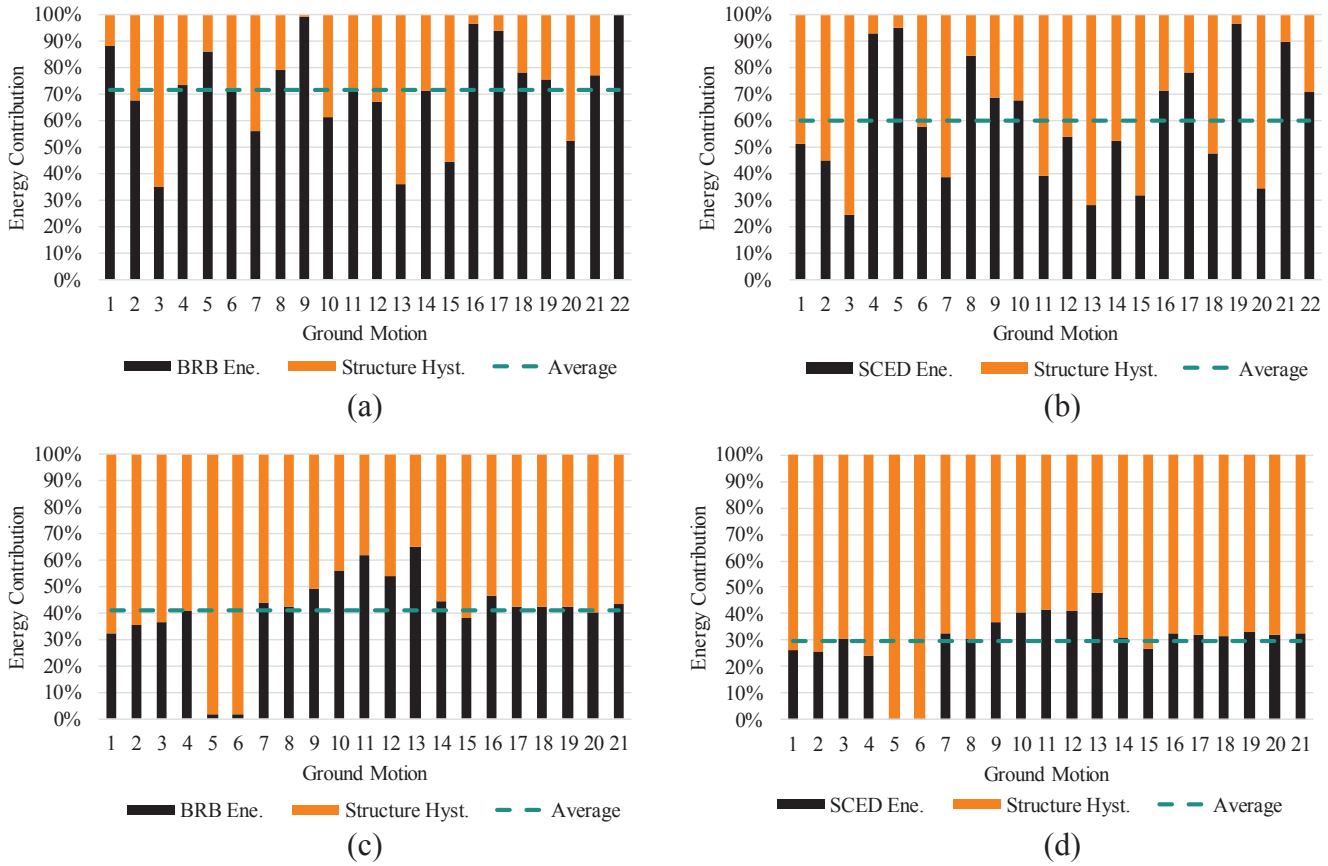


**Fig. 10.** Energy dissipation contribution in bridge retrofitted with: (a) BRBs under FFGMs, (b) SCEDs under FFGMs, (c) BRBs under PTGMS, and (d) SCEDs under PTGMs.

bent, with no external energy dissipation devices, the input energy is transformed to kinetic energy, recoverable elastic strain (strain energy), and is also dissipated through structural material damping (damping energy) and irrecoverable inelastic strain (hysteretic energy). External energy dissipation devices reduce inelastic strain in the structure by dissipating earthquake input energy, creating a structural fuse. The high energy dissipation in BRBs leads to lower peak drift ratios, and hence lower inelastic deformations. The trade-off of using SCEDs to achieve lower residual drift ratios is reduced energy dissipation thus leading to slightly higher peak drift ratios as compared to BRB retrofitted structures.

### 6.1. Incremental dynamic analysis

Fragility curves were developed for the as-built and retrofitted bridge bents by performing Incremental Dynamic Analyses (IDAs) [48]. The IDA is a numerical analysis procedure that correlates the structure's performance in terms of the engineering demand parameter (*EDP*) selected as the peak drift ratio (%) to a ground motion input parameter, the Intensity Measure (*IM*). In this study, the 5% damped first mode spectral acceleration, $Sa(T_1)$[g] was selected as the *IM*. The drift ratio was selected as the *EDP* because it correlates with the bridge bent damage states using pushover analysis, as shown Table 3. Scaling ground motions using spectral acceleration results in lower dispersion in the output parameter values [49,50]. The selected FFGMs (Table 4) and PTGMs (Table 5) were monotonically increased at 0.1 g intervals to

obtain the structural response from elastic behavior until the occurrence of structural failure. In addition to the damage state limits defined previously, structural collapse was assumed when the structure attained very large peak drift ratios for consecutive *IM* values, i.e. when the IDA curves become horizontally asymptotic.

At a chosen intensity measure, the probability that the seismic demand ($D$) of the bridge bent exceeds its capacity ($C|IM$) can be assessed by fragility curves. A lognormal distribution of demand and capacity is assumed, and the probability of reaching or exceeding a specific damage state for a particular component is then estimated using the probability equation, Eq. (6), and the dispersion value ($\beta$), Eq. (7):

$$P[D > C|IM] = \Phi\left[\frac{\ln(IM) - \ln(\alpha)}{\sqrt{\beta_{D|IM}^2 + \beta_C^2}}\right] \tag{6}$$

$$\beta_{D|IM} = \sqrt{\frac{\sum_1^N [\ln(D_i) - \ln(M)]^2}{N-1}} \tag{7}$$

where $\alpha$ is the median estimate of the capacity, $\beta_C$ is the dispersion of the capacity, $\Phi(*)$ is the standard normal cumulative distribution function, $D_i$ is the seismic demand for a particular ground motion, $M$ is the median value of the seismic demand, and $N$ is the total number of data points.

Fig. 11 compares IDA and fragility curves for the as-built bridge bent, and the bents retrofitted with BRBs or SCEDs for the 22 FFGMs. The dispersion ($\beta$) and median values ($S_D$) for each performance limit state fragility curve are provided in Table 6. The median spectral acceleration of exceeding the "slight" damage state was 0.33 g for the as-built condition, which was enhanced to 0.66 g for the bridge bent with the BRB retrofit and 0.62 g for the bridge bent with the SCED retrofit. The spectral acceleration for the median probability of exceeding the "Moderate" damage state for the as-built bridge bent was 1.20 g, which was improved to 2.20 g for the BRB retrofit and 2.10 g for the SCED retrofit. Similarly, the spectral acceleration for the median probability of exceeding the "Extensive" damage state improved from 1.50 g for the as-built bridge bent to 2.70 g for the BRB retrofit and 2.49 g with the SCED retrofit. For the three damage states, the BRB retrofit was more effective than the SCED retrofit, because the BRBs show cyclic strain hardening that enables them to resist a higher load and dissipate more energy. Since the performance of BRB and SCED retrofitted bents was very close, a pairwise comparison approach was used for evaluating the IDA curves at different limit states. The results show that the improved performance of the BRB retrofit versus SCED retrofit in the case of slight, moderate, and extensive limit states is statistically significant. The difference between the performance of the two retrofit systems in improving the collapse limit was found to be not statistically significant, as also demonstrated in Table 6.

The results for IDA using PTGMs for the as-built and retrofitted bridge bents are presented in Fig. 12. The dispersion in results for slight, moderate, and extensive damage limit states is larger under PTGMs than under FFGMs, as shown in Table 7. The median probability values show that the BRB and SCED retrofits improved the bent performance by more than two times (0.70 g and 0.68 g, respectively) for the "Slight" damage limit as compared to the as-built bridge bent (0.30 g). For the "Moderate" damage state, the capacity of the bent was improved by 1.50 and 1.45 times for the BRB and the SCED retrofit, as compared to the as-built condition. Similarly, for the "Extensive" damage state, the capacity of the bent was improved by 1.44 and 1.41 times for the BRB and SCED retrofit, respectively, as compared to the as-built condition. As observed from the median $Sa(T_1)$[g] values in Tables 6 and 7, the improvement provided by the braces was higher for FFGMs than for PTGMs. When the bent is excited by multiple large cycles under a FFGM, the input energy is dissipated by the braces through hysteretic behavior. However, under PTGMs the braces work more like additional stiffness-providing members, rather than energy dissipation components; once they yield or are activated, they tend to deform to a larger extent under the influence of a single strong pulse. Hence, the performance improvement under PTGMs is not as efficient as for FFGMs. A pairwise comparison test was performed on the IDA data for the two retrofitted bents subjected to PTGMs. The t-values for slight, moderate and extensive damage limit states ranged between 2.406 and 2.448 making the results statistically significant. The performance difference between the two retrofit schemes was found to be not statistically significant for the collapse limit state.

On the other hand, the SCED retrofit is more efficient at reducing the residual drift ratio. Based on the quasi-static cyclic hysteresis of the as-built bridge bent, shown in Fig. 13(a), the *possible range* of the residual drift ratio can be estimated as ($\Delta_{res}^{+}$, $\Delta_{res}^{-}$). This range is based on the bounds of bent drift ratio when the base shear is zero in cyclic or dynamic analysis. The bridge bent residual drift ratio is caused by large inelastic deformation in the core concrete and large inelastic strains in the column longitudinal steel reinforcement. When equipped with BRBs, this residual drift can also be caused by residual deformation of the BRB steel core. Once the column core concrete is damaged, excessive yielding and/or buckling of the longitudinal steel reinforcement occurs, leading to larger residual drifts. The actual residual drift depends on the bridge's displacement time history, which varies based on the input ground motion. This *actual* residual drift exists between the absolute bounds of the *possible range* of residual drift ($\Delta_{res}^{-} < \Delta_{actual} < \Delta_{res}^{+}$) due to dynamic effects. Fig. 13(b) shows a comparison between the most probable and absolute residual drift ratio for a representative FFGM (Kobe 1995). The drift time-histories of the as-built and retrofitted bents are compared in Fig. 13(c) for the Kobe (1995) FFGM scaled to $S_a[T_1]$ = 1.5, 2.0, and 3.0 g. For the as-built bridge, the analysis failed to converge when $S_a[T_1]$ = 3.0 g. The bridge bent retrofitted with BRBs reduced the peak and residual drift ratio as compared to the as-built condition, but showed high residual drift ratios for ground motions with high spectral accelerations. The SCED retrofit significantly reduced the residual drift ratio of the bridge bent even for ground motions with high spectral accelerations.

A probabilistic approach using IDA was implemented to evaluate the performance of the retrofitted bridge bent in the context of residual drift ratio. The residual drift ratio of the bent was considered as the *EDP* and the first period spectral acceleration, $S_a(T_1)$[g], was considered as the *IM*. A vertical CDF was plotted up to a 0.5% residual drift ratio on the horizontal axis to show the distribution of ground motion *IM* required to exceed the "serviceability limit". A CDF of ground motion *IM* required to exceed a residual drift ratio of 0.5% for the as-built and retrofitted bents is shown in Fig. 13(d). The as-built bridge bent had a 50% probability of exceeding the "serviceability limit" of residual drift ratio at a spectral acceleration of 2.02 g. The BRB retrofitted bridge bent met serviceability requirements up to a median spectral acceleration of 3.00 g, and the SCED retrofitted bridge up to 4.67 g. The SCED pretensioned bars/tendons remained elastic up to a 3.23% drift ratio of the bridge bent, providing the re-centering force to keep the bridge "serviceable" for an input acceleration up to 4.67 g.

Application of replaceable energy dissipation devices in bridge bents offers lifetime cost benefits by limiting structural damage during large earthquakes. Reducing residual drift in the structure by using SCEDs makes it convenient to replace them, thus further reducing the cost of bringing the structure back to the original position after an earthquake. Further details on the cost-benefit of using BRBs, SCEDs and other seismic retrofit systems in bridge structures can be found elsewhere [10,11,51–53].

## 7. Conclusions

This paper presents numerical simulations of a structurally deficient bridge bent retrofitted with buckling restrained braces (BRBs) or self-centering energy dissipation devices (SCEDs). The numerical models of the as-built bridge bent, the BRB component, and the SCED component

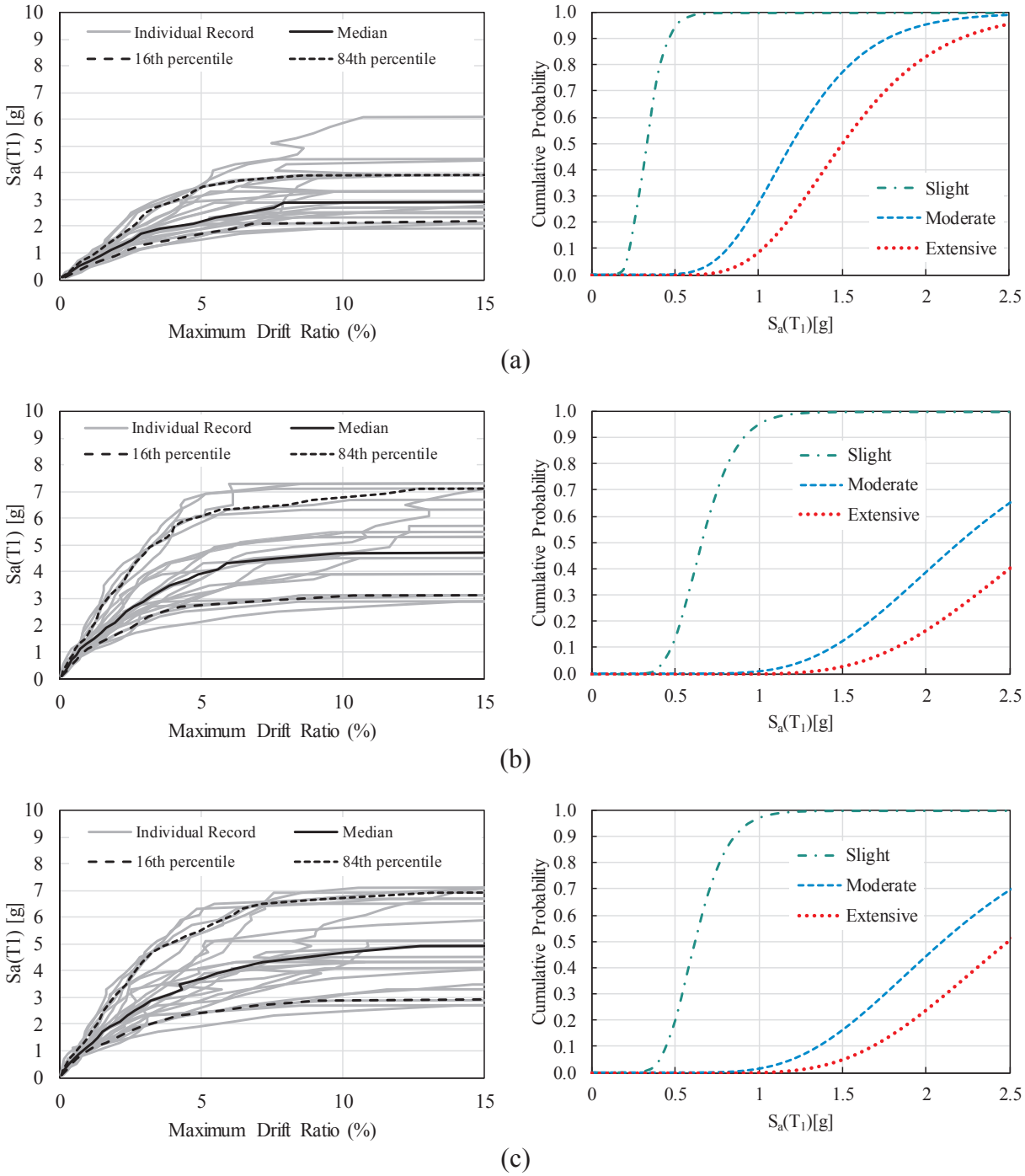


**Fig. 11.** IDA and fragility curves for 22 far-field ground motions: (a) as-built bent; (b) BRB retrofitted bent; and (c) SCED retrofitted bent.

**Table 6**
Parameters of fragility curves for as-built and retrofitted bridge bents with respect to spectral acceleration for far-field ground motions.

| Bridge Condition | Slight | | Moderate | | Extensive | | Collapse | |
|---|---|---|---|---|---|---|---|---|
| | $\beta$ | M (g) | $\beta$ | M (g) | $\beta$ | M (g) | $\beta$ | M (g) |
| As-Built | 0.26 | 0.33 | 0.30 | 1.20 | 0.30 | 1.50 | 0.24 | 3.67 |
| BRB Retrofit | 0.25 | 0.66 | 0.33 | 2.20 | 0.31 | 2.70 | 0.30 | 5.01 |
| SCED Retrofit | 0.25 | 0.62 | 0.34 | 2.10 | 0.31 | 2.49 | 0.30 | 5.04 |

developed in OpenSees were validated using previous experimental results. A distributed plasticity fiber model was used to predict the seismic performance of the as-built and retrofitted bridge bents which was compared using a probabilistic approach. Fragility curves were developed using incremental dynamic analysis (IDA) to assess the impact of a BRB or SCED seismic retrofit. The following conclusions were reached:

1. The numerical model of the as-built bridge bent was validated using experimental results of an in-situ cyclic test of a full-scale bridge. The numerical model included longitudinal reinforcement buckling and was able to reproduce the drift ratios corresponding to various damage states observed in the in-situ test.

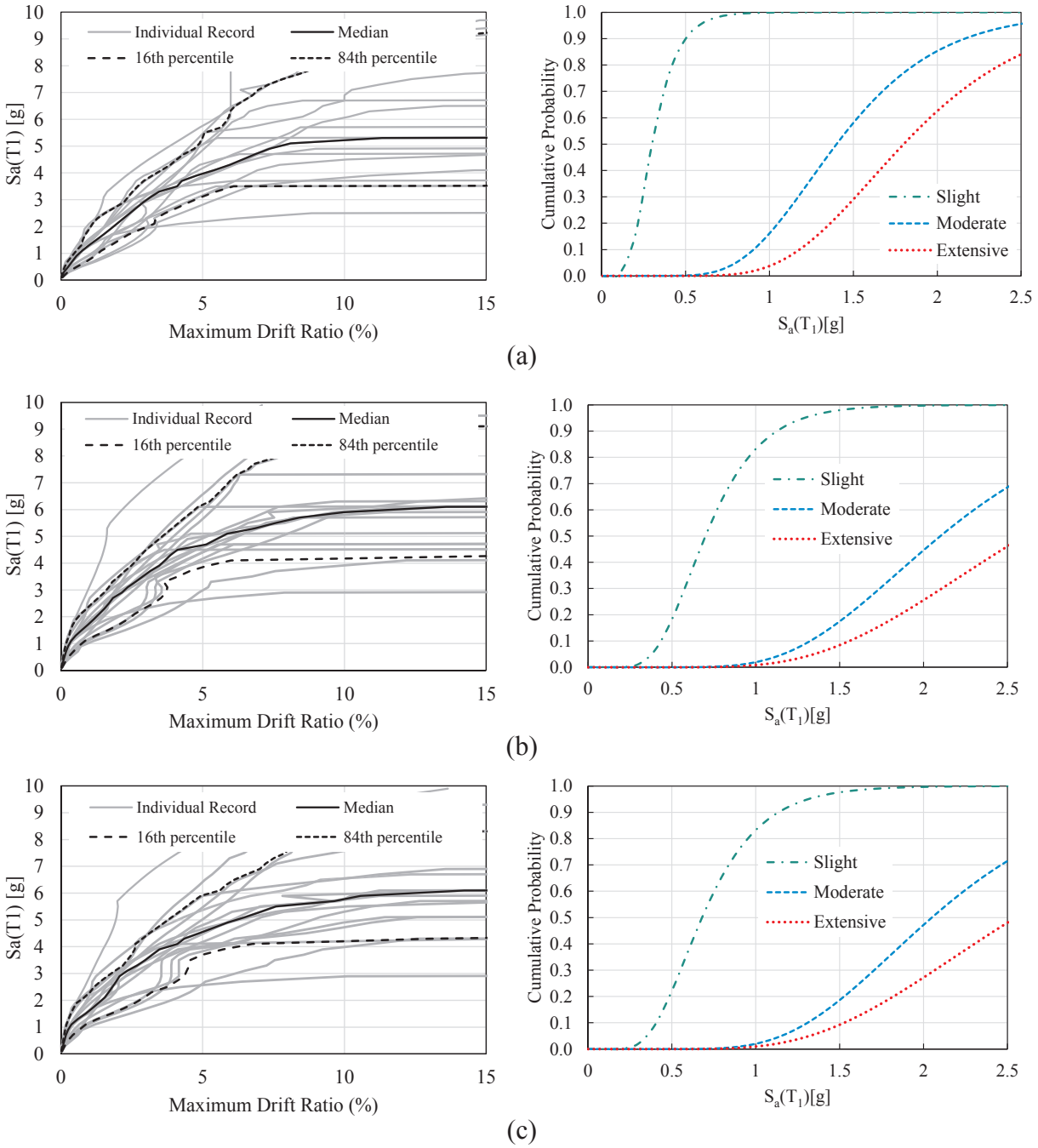


**Fig. 12.** IDA and fragility curves for 21 pulse-type ground motions: (a) as-built; (b) BRB retrofitted bent; and (c) SCED retrofitted bent.

**Table 7**
Parameters of fragility curves for as-built and retrofitted bridge bents with respect to spectral acceleration for pulse-type ground motions.

| Bridge Condition | Slight | | Moderate | | Extensive | | Collapse | |
|---|---|---|---|---|---|---|---|---|
| | $\beta$ | M (g) | $\beta$ | M (g) | $\beta$ | M (g) | $\beta$ | M (g) |
| As-Built | 0.40 | 0.30 | 0.34 | 1.40 | 0.33 | 1.80 | 0.30 | 5.81 |
| BRB Retrofit | 0.37 | 0.70 | 0.36 | 2.10 | 0.40 | 2.60 | 0.26 | 6.40 |
| SCED Retrofit | 0.40 | 0.68 | 0.35 | 2.05 | 0.40 | 2.55 | 0.29 | 6.44 |

2. BRBs or SCEDs work as structural fuses that dissipate seismic input energy and provide additional stiffness to the bridge bent. The BRB component model could reproduce BRB cyclic tests including cyclic strain hardening and fatigue failure with reasonable accuracy, with a maximum error of 2% in the cumulative hysteretic energy dissipated compared to cyclic tests of the brace. The SCED component numerical model predicted the initial stiffness, peak force, and re-centering accurately, with a maximum error of 2% in the total hysteretic energy dissipated when validated against a cyclic test of the device.
3. The peak drift ratio demand of the as-built bridge bent for pulse-type ground motions (PTGMs) scaled to the Maximum Considered Earthquake (MCE) was generally lower that the peak drift ratio obtained for far-field ground motions (FFGMs) due to the larger cyclic degradation and damage to the structure triggered by multiple large cycles inherent in FFGMs.
4. When subjected to FFGMs scaled to the MCE level, the median value of peak drift ratio demand experienced by the bridge bent was

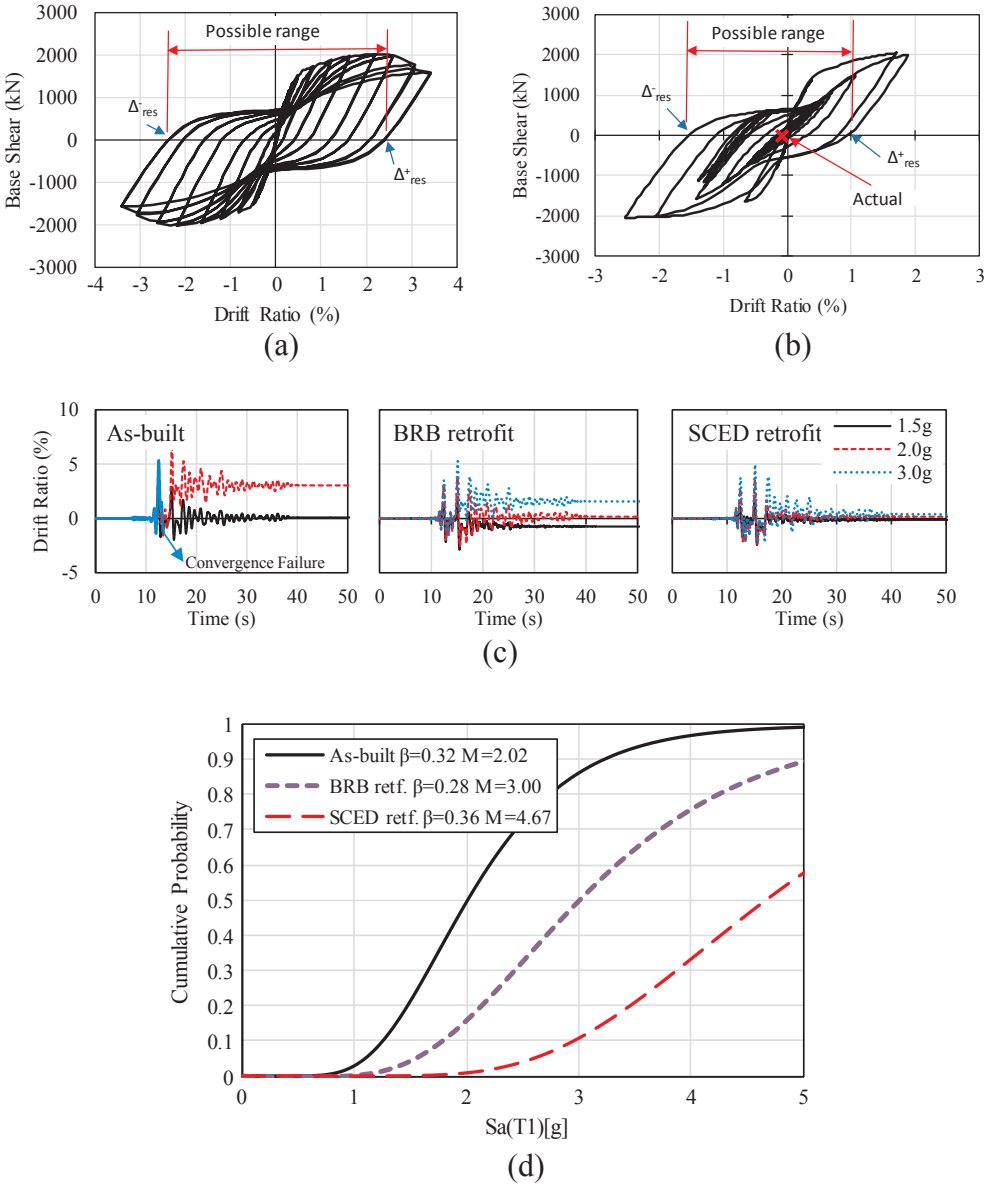


**Fig. 13.** Residual drift performance: (a) residual drift estimation in cyclic loading; (b) effect of dynamic loading on residual drift; (c) effect of retrofit for Kobe (1995) scaled to 1.5 g, 2.0 g and 3.0 g; (d) CDFs for serviceability residual drift ratio (0.5%) in as-built and retrofitted bridge bents for far-field and pulse-type ground motions.

reduced to 0.63% for the retrofitted structure with BRBs and 0.70% for the retrofitted structure with SCEDs, compared to 1.50% for the structure in the as-built condition. For PTGMs scaled to the MCE level, the median peak drift ratio demand was reduced from 1.26% for the as-built condition to 0.62% for both the BRB and the SCED retrofitted bridge bents.

5. The residual drift demand for the as-built bridge bent was generally higher for FFGMs than for PTGMs. For FFGMs scaled to MCE level, the bridge bent had an 82% probability of remaining serviceable (residual drift ratio less than 0.5%) for the as-built condition; this was enhanced to 94% for the BRB retrofitted structure and 100% for the structure with the SCED retrofit. When subjected to PTGMs scaled to the MCE level, the bridge bent had an 87% probability of remaining serviceable for the as-built condition; this was enhanced to 96% for the bridge bent with the BRB retrofit, and 100% for the bridge bent with the SCED retrofit. The performance of the BRB and SCED retrofits in lowering peak drift ratio demand when subjected to MCE level pulse-type ground motions was found to be very close.
6. Incremental Dynamic Analysis (IDA) showed that BRBs are more effective in reducing the bent peak drift ratio demand under FFGMs than under PTGMs. Both the BRB and SCED retrofit techniques showed comparable effectiveness in enhancing the bridge bent performance for “slight” and “moderate” damage limits. For the “extensive” damage limit, the BRB retrofit was more effective than the SCED retrofit for FFGMs, while the two retrofit techniques showed similar performance when subjected to PTGMs.
7. For a bridge bent with substandard seismic details, the SCED retrofit showed significant advantage in mitigating residual drifts over the BRB retrofit for ground motions larger than the Design Basis Earthquake. This is an important parameter for maintaining post-earthquake serviceability, thus increasing bridge resilience and keeping repair costs low.

Further research is needed to investigate the performance of connections of BRB/SCED to bridge columns or foundations. In addition, further study is required to assess the influence of boundary conditions

and soil conditions on the fragility of BRB and SCED retrofit methods in multi-column bridge bents.

## Declaration of Competing Interest

The authors declared that there is no conflict of interest.

## Acknowledgements

The work presented in this paper was conducted with support by the University of Utah and the Mountain-Plains Consortium [Grant No. MPC-491], a University Transportation Center funded by the U.S. Department of Transportation. The contents of this paper reflect the views of the authors, who are responsible for the facts and accuracy of the information presented.

## References

[1] USDOT. National Transportation Statistics. U.S. Department of Transportation, Bureau of Transportation Statistics. Washington (D.C.); 2014.
[2] Hsu YT, Fu CC. Seismic effect on highway bridges in Chi Chi earthquake. J Perform Constructed Facil 2004;18(1):47–53. https://doi.org/10.1061/(ASCE)0887-3828(2004) 18:1(47).
[3] Fujino Y, Hashimoto S, Abe M. Damage analysis of Hanshin Expressway viaducts during 1995 Kobe earthquake. I: residual inclination of reinforced concrete piers. J Bridge Eng 2005;10(1):45–53.
[4] Abe M, Shimamura M. Performance of railway bridges during the 2011 Tohoku earthquake. J Perform Constructed Facil 2012;28(1):13–23.
[5] Basoz NI, Kiremidjian AS, King SA, Law KH. Statistical analysis of bridge damage data from the 1994 Northridge, CA, earthquake. Earthquake Spectra 1999;15(1):25–54.
[6] Yashinsky M. Performance of bridge seismic retrofits during Northridge earthquake. J Bridge Eng 1998;3(1):1–14.
[7] Sun C, Xu J. Estimation of time for Wenchuan earthquake reconstruction in China. J Constr Eng Manage 2010;137(3):179–87.
[8] El-Bahey S, Bruneau M. Buckling restrained braces as structural fuses for the seismic retrofit of reinforced concrete bridge bents. Eng Struct 2011;33(3):1052–61.
[9] Upadhyay A, Pantelides CP, Ibarra L. Seismic performance of curved bridges on soft soils retrofitted with buckling restrained braces. Phoenix, Arizona: ASCE; 2015.
[10] Bazaez R, Dusicka P. Cyclic behavior of reinforced concrete bridge bent retrofitted with buckling restrained braces. Eng Struct 2016;119:34–48. https://doi.org/10.1016/j.engstruct.2016.04.010.
[11] Bazaez R, Dusicka P. Performance assessment of multi-column RC bridge bents seismically retrofitted with buckling-restrained braces. Bull Earthq Eng 2017;16(5):2135–60. https://doi.org/10.1007/s10518-017-0279-3.
[12] Upadhyay A, Pantelides CP. Comparison of the seismic retrofit of a three-column bridge bent with buckling restrained braces and self centering braces. Structures congress 2017 Denver, Colorado: American Society of Civil Engineers; 2017. p. 414–23. https://doi.org/10.1061/9780784480403.035.
[13] Wang Y, Ibarra L, Pantelides C. Seismic retrofit of a three-span RC bridge with buckling-restrained braces. J Bridge Eng 2016;21(11):04016073. https://doi.org/10.1061/(ASCE)BE.1943-5592.0000937, 04016073.
[14] Fahnestock L, Ricles J, Sause R. Experimental evaluation of a large-scale buckling-restrained braced frame. J Struct Eng 2007;133(9):1205–14. https://doi.org/10.1061/(ASCE)0733-9445(2007) 133:9(1205).
[15] Ariyaratana C, Fahnestock LA. Evaluation of buckling-restrained braced frame seismic performance considering reserved strength. Eng Struct 2011;33(1):77–89. https://doi.org/10.1016/j.engstruct.2010.09.020.
[16] Erochko J, Christopoulos C, Tremblay R, Choi H. Residual drift response of SMRFs and BRB frames in steel buildings designed according to ASCE 7–05. J Struct Eng 2011;137(5). https://doi.org/10.1061/(ASCE)ST.1943-541X.0000296.
[17] Chou CC, Chen Y, Pham D, Truong V. Steel braced frames with dual-core SCBs and sandwiched BRBs: mechanics, modeling and seismic demands. Eng Struct 2014;72(1):26–40.
[18] Kamulla V, Erochko J, Kwon O, Christopoulos C. Application of hybrid-simulation to fragility assessment of the telescoping self-centering energy dissipative bracing system. Earthq Eng Struct Dyn 2014;43:811–30.
[19] Dong H, Du X, Han Q, Hao H, Bi K, Wang X. Performance of an innovative self-centering buckling restrained brace for mitigating seismic responses of bridge structures with double-column piers. Eng Struct 2017;148:47–62. https://doi.org/10.1016/j.engstruct.2017.06.011.
[20] Christopoulos C, Tremblay R, Kim H, Lacerte M. Self-centering energy dissipative bracing system for the seismic resistance of structures: development and validation. J Struct Eng 2008;134(1):96-107. https://doi.org/10.1061/(ASCE)0733-9445(2008)134:1(96).
[21] Chou C, Chung P. Development of cross-anchored dual-core self-centering braces for seismic resistance. J Constr Steel Res 2014;101:19–32. https://doi.org/10.1016/j.jcsr.2014.04.035.
[22] Zhou Z, He XT, Wu J, Wang CL, Meng SP. Development of a novel self-centering buckling-restrained brace with BFRP composite tendons. Steel Comp Struct 2014;16(5):491–506.
[23] Miller DJ, Fahnestock LA, Eatherton MR. Development and experimental validation of a nickel-titanium shape memory self-centering buckling-restrained brace. Eng Struct 2012;40:288–98.
[24] Pantelides CP, Gergely I, Reaveley L, Volnyy VA. Retrofit of R/C bridge pier with CFRP advanced composites. J Struct Eng 1999;125(10):1094–9.
[25] Pantelides CP, Reaveley L, Duffin J, Ward J, Delahunty C. In-situ tests of three bents at South Temple Bridge on Interstate 15 – Final report. Utah Department of Transportation Research Division. Report No. UT-03.32, Utah; 2003.
[26] Pantelides CP, Ward JP, Reaveley LD. Behavior of R/C bridge bent with grade beam retrofit under simulated earthquake loads. Earthquake Spectra 2004;20(1):91–118.
[27] Pantelides CP, Duffin JB, Reaveley LD. Seismic strengthening of reinforced-concrete multicolumn bridge piers. Earthquake Spectra 2007;23(3):635–64.
[28] Gergely I, Pantelides CP, Reaveley LD. Shear strengthening of R/C T-joints using CFRP composites. J Compos Constr 2000;4(2):56–64.
[29] Pantelides CP, Fitzsimmons G. Case study of strategies for seismic rehabilitation of reinforced concrete multicolumn bridge bents. J Bridge Eng 2012;17(1):139–50. https://doi.org/10.1061/(ASCE)BE.1943-5592.0000203.
[30] McKenna F. Open system for earthquake engineering simulation (OpenSees). Berkeley: California; 2014.
[31] Kunnath SK, Heo Y, Mohle JF. Nonlinear uniaxial material model for reinforcing steel bars. J Struct Eng 2009;135(4):335–43.
[32] Dhakal RP, Maekawa K. Modeling for Postyield buckling of reinforcement. J Struct Eng 2002;128(9):1139–47. https://doi.org/10.1061/(ASCE)0733-9445(2002) 128:9(1139).
[33] Mahrenholtz C, Lin P, Wu A, Tsai K, Hwang S, Lin R, et al. Retrofit of reinforced concrete frames with buckling-restrained braces. Earthq Eng Struct Dyn 2015;44:59–78. https://doi.org/10.1002/eqe.2458.
[34] ASCE. Minimum design loads for buildings and other structures. ASCE/SEI 7-10, Reston, VA; 2013.
[35] Uriz P. Towards Earthquake resistant design of concentrically braced steel structures Doctoral Dissertation Berkeley (CA): Department of Civil and Environmental Engineering, University of California; 2005.
[36] Xu W, Pantelides CP. Strong-axis and weak-axis buckling and local bulging of buckling-restrained braces with prismatic core plates. Eng Struct 2017;153:279–89.
[37] Black CJ, Makris N, Aiken ID. Component testing, seismic evaluation and characterization of buckling-restrained braces. J Struct Eng 2004;130(6):880–94.
[38] Zona A, Dall'Asta A. Elastoplastic model for steel buckling-restrained braces. J Constr Steel Res 2012;68:118–25.
[39] Krawinkle H, Zareian F, Medina RA, Ibarra L. Contrasting performance-based design with performance assessment. International workshop on performance-based seismic design, Bled, Slovenia. 2004. ISBN 0-9762060-0-5.
[40] HAZUS-MH. Multi-Hazard Loss Estimation Methodology: Earthquake Model. Washington DC. Department of Homeland Security, FEMA; 2003.
[41] FEMA. NEHRP Recommended Seismic Provisions, FEMA P-695. Federal Emergency Management Agency, Washington (D.C.); 2009.
[42] USGS. Seismic Design Map Tools. US Geological Survey; 2014. http://earthquake.usgs.gov/designmaps/us/application.php.
[43] PEER. NGA-West2 database flat-file, Pacific Earthquake Engineering Research Center. Available: http://peer.berkeley.edu/ngawest2/databases/ [last accessed 14 August 2016].
[44] OES. Vision 2000: Performance Based Seismic Engineering of Buildings", Prepared by Structural Engineers Association of California. California Office of Emergency Services. CA; 1995.
[45] Benjamin JR, Cornell CA. Probability, statistics, and decision for civil engineers. New York: McGraw-Hill; 1970.
[46] Dhakal RP, Singh S, Mander JB. Effectiveness of earthquake selection and scaling method in New Zealand. Bull NZ Soc Earthquake Eng 2007;40(3).
[47] Uang C, Bertero VV. Evaluation of seismic energy in structures. Earth Eng Struct Dyn 1990;19:77–90.
[48] Vamvatsikos D, Cornell CA. Incremental dynamic analysis. Earthq Eng Struct Dyn 2002;31(3):491–514.
[49] Baker JW, Cornell CA. Vector-valued ground motion intensity measures or probabilistic seismic demand analysis. Pacific Earthquake Engineering Research Rep. 2006/08, Pacific Earthquake Engineering Research Center, Univ. of California, Berkeley, CA; 2006.
[50] Zareian F, Krawinkler H, Ibarra L. Why and how to predict the probability of collapse of buildings. 8th U.S national conference on earthquake engineering, San Francisco (CA). 2006.
[51] Cheng Xi. Improving the Seismic Performance of Existing Bridge Structures Using Self-Centering Dampers. Doctoral Thesis published in Library Catalogue Record, Carleton University; 2017. doi: http://doi.org/10.22215/etd/2017-11966.
[52] Gallardo Bazáez, Gabriel Ramiro Andrés. Achieving Operational Seismic Performance of RC Bridge Bents Retrofitted with Buckling-Restrained Braces. Dissertations and Theses. Paper 3476; 2017. doi: http://doi.org/10.15760/etd.3352.
[53] Miotke Michael K. Seismic Retrofit Case Study of Reinforced Concrete Bridges with Buckling Restrained Braces. Civil and Environmental Engineering Master's Project Reports. 33; 2017.